MACHINE DESIGN, VOL.12(2020) NO.4, ISSN 1821-1259 PP. 89-94

DOI: 10.24867/MD.12.2020.4.89-94
Research paper

FEM MODELLING OF INTERACTION BETWEEN WHEEL AND ASPHALT

Marko TOPALOVIĆ[1, *], Vladimir MILOVANOVIĆ[2], Nikola JOVIĆ[2], Ljudmila KUDRJAVCEVA[3], Milan MIĆUNOVIĆ[2]
[1] University of Kragujevac, Institute for Information Technologies, Kragujevac, Serbia,
[2] University of Kragujevac, Faculty of Engineering, Kragujevac, Serbia,
[3] The State University of Novi Pazar, Serbia

Received (30.09.2020); ***Revised*** (26.11.2020); ***Accepted*** (28.11.2020)

Abstract: *Experimental analysis of the asphalt samples and numerical models of these experiments found in literature, are performed using the various rates of deformations, range of temperatures, and a spectrum of loading cycles. Results obtained from these experiments and simulations characterize asphalt in the laboratory conditions. However, the interaction between the wheel and the asphalt is much more complex, rate of deformation depends on vehicle velocity, load, tire properties. In this paper, we present a modeling of rolling motion of a wheel over the asphalt pavement using the Finite Element Method (FEM). The goal presented in this paper is the determination of the appropriate rate of deformation using realistic model, which will be used afterwards in the experiments, or numerical models of asphalt specimens. Load definition, prescribed displacements, kinematic constraints, and contact enforcement are given.*

Key words: *Asphalt model, FEM analysis, kinematic constraints, rolling motion, wheel*

1. INTRODUCTION

The Hot Mix Asphalt (HMA) is heterogeneous, visco-elastoplastic, temperature dependent, anisotropic material [1] which composition and properties are tailored to meet specific requirements derived from the local weather and climate conditions [2]. Developing a unified material model for HMA has been proven difficult and is still a work in progress [3]. Due to the presence of a viscous bitumen binder, asphalt behavior is deformation rate dependent, and bitumen viscosity is related to the temperature. However, experimental testing of the asphalt samples is performed by researchers using the regional asphalt samples with local temperature ranges [4]. HMA consists of gravel and sand grains (aggregates), and they made up 93-97% of the volume, while the rest of the volume is bitumen binder. Sand and gravel are granular materials [5], which means that the bigger grains in contact form force chains which carry most of the load while the smaller grains have a supporting role. Granular materials exhibit dilatation, i.e. volumetric expansion due to the saw-like rearranging of the grains during the shear. Figure 1 shows the asphalt composition, force chains and the dilatation.

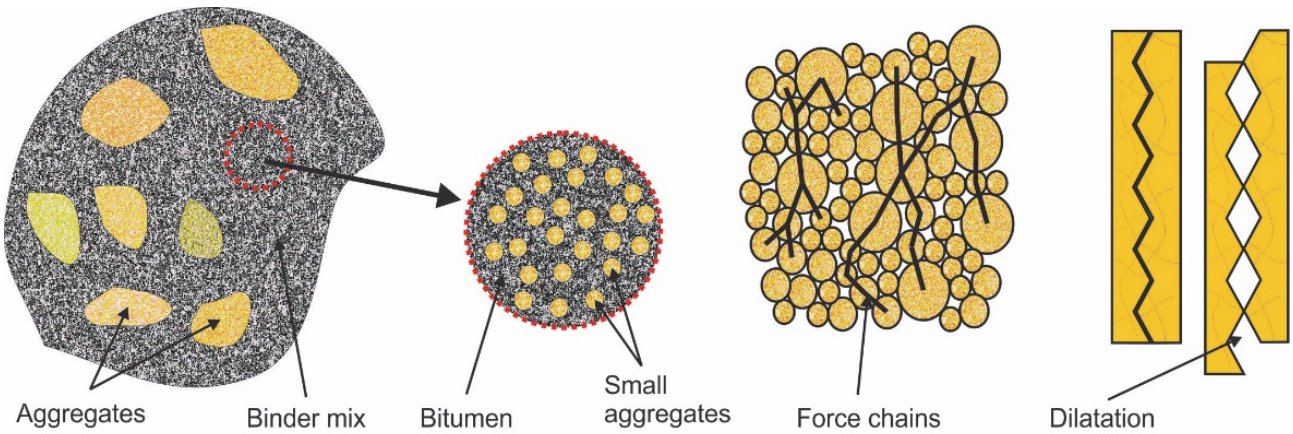

Fig.1. Hot Mix Asphalt composition, granular material force chains and dilatation

Rutting is the most common damage in HMA caused by the shear stress that occurs at the edges of the contact surface between wheel and pavement [6]. In the most simplified case, when the deformations of pavement and the wheel are neglected, we would calculate the total weight of the vehicle that each wheel carries, and distribute it across the contact as nodal forces. If we take into a consideration only the tire deformation, then we would need to know the area of the contact surface and the pressure distribution within the contact. The most realistic case, (which is used in this paper) implies deformations of both tire and the asphalt. In the Figure 2, simplified and realistic models of wheel-asphalt contact are given, and rutting is shown.

*Correspondence Author's Address: University of Kragujevac, Institute for Information Technologies, Jovana Cvijića bb, 34000 Kragujevac, Serbia, topalovic@kg.ac.rs

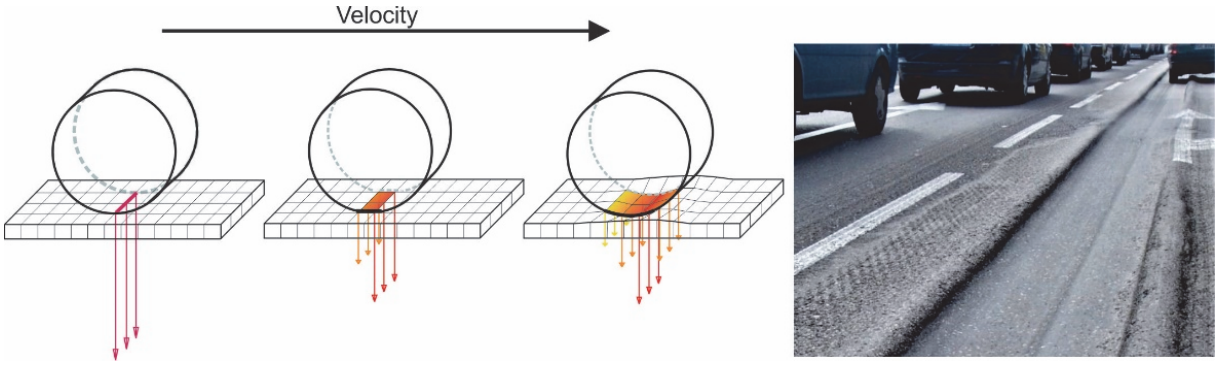

a) *b)*

Fig.2. a) Simplified and realistic models od wheel-asphalt contact b) rutting

2. MODELLING OF WHEEL MOTION AND CONTACT WITH ASPHALT

In order to have the most realistic model, we must take into consideration rolling of the wheel as well, but due to the nature of the FEM, especially contact algorithm, this has been a true challenge. One would expect that the sufficient constraints would be to prescribe horizontal motion of the wheel axis, and that the wheel would rotate due to the contact with the surface, or to prescribe rotation of the wheel, and that this rotation would cause translation of the wheel. But, this is not the case, both rotation and translation need to be prescribed, and in this paper, we will focus on why, and how to do this.

FEM modelling was done in FEMAP pre and post-processing software [7]. Since the general goal of our research is to develop a unified material model for HMA which would be applicable for all of the composition and temperature combinations, we had to use a few FEM solvers along the way. First we started with the ABAQUS, since it allows the new material model to be added as a user subroutine, and it has advantages in terms of availability of contact mechanics algorithms and simplicity of implementation, but the disadvantages of ABAQUS were also great, such as storing the variables from previous step, and inadequate capabilities for thermal analysis [8]. Then we switched to the in-house developed FEM program called PAK-Multiphysics developed by the Laboratory for Engineering Software, Faculty of Engineering, University of Kragujevac [9]. Access to the PAK source code allows us full control of thermo-mechanical coupling and easy access to all required variables, but PAK lacks some of the features available in the state of the art commercial software. Now, our methodology implies that we first make a FEM model of rolling wheel in FEMAP, then use the built-in ADINA solver to test load, constraint and contact definition, and to determine proper loading function. Finally, we used this loading function on a simplified model of experiment specimen on which we can test a new material model for asphalt.

The contact algorithms in the most FEM solvers clearly identify master/ target surface and slave/contactor surface (names vary between solvers, but the function is the same). Usually master surface is larger, stiffer and have coarser mesh than the slave surface. In our case of the wheel to asphalt contact, wheel should be a slave and asphalt the master. Contact algorithms determine penetration of slave nodes into the master surface, and based on that penetration, repulsive contact force is calculated. Depending on the geometry, repulsive contact force can have both normal and tangential component, but the tangential component of the contact force alone cannot cause the realistic rotation of the wheel, because it is based on the theory which defines sliding of one surface over the other. In our case, sliding between slave wheel nodes and master asphalt surface would only cause stretching of the tire in contact with the asphalt, so we needed the different approach for rotation prescription. Kinematically, rotation of the wheel is dependent on the vehicle velocity and the wheel radius ( ), so the most practical solution is to prescribe rotation around the axis, alongside previously defined horizontal translation of the axis. If we prescribe displacement of the FEM nodes that lay on the axis, the whole wheel slides across the asphalt as the axis node displacements are propagated throughout the wheel mesh. However, we cannot do the same with the rotation, because we cannot prescribe rotation of the points, we must somehow define the rotation of the elements instead. In FEM, rotation of the elements is achieved through tangential displacement of nodes, so if we would to prescribe rotation of the all wheel elements, we would get completely rigid wheel which could not deform under vehicle weight as all of the node displacements would be constrained by the prescribed rotation.

The solution is to prescribe only the rotation of the rim, and to leave the tire elements free to deform under vehicle weight and contact with the pavement. This way, the rotation of the rim would propagate to the tire elements, and we get realistic behavior.

To prescribe rotation of rim elements around wheel axis, i.e. to define kinematic constraints of their nodes, we used so called “spider elements”. These are artificial, rigid connections that consist of one point (node) for which the constraints/loads are defined, and many related, connected nodes which have the same constraints/loads as the center node are shown in Figure 3. a). Alternatively, in order to use FEM solver which does not have spider elements, we had to use existing beam elements with coupled constrains, so they behave the same way as the rigid elements in the spider connection. To create these beam elements, we developed FEMAP API function [7] which creates beam elements from selected rim nodes and generates center node for prescription of displacement and rotation. Now we must connect all the outer nodes of beam elements with central node using Mesh>Connect>Closest Link command shown in Figure 3. b).

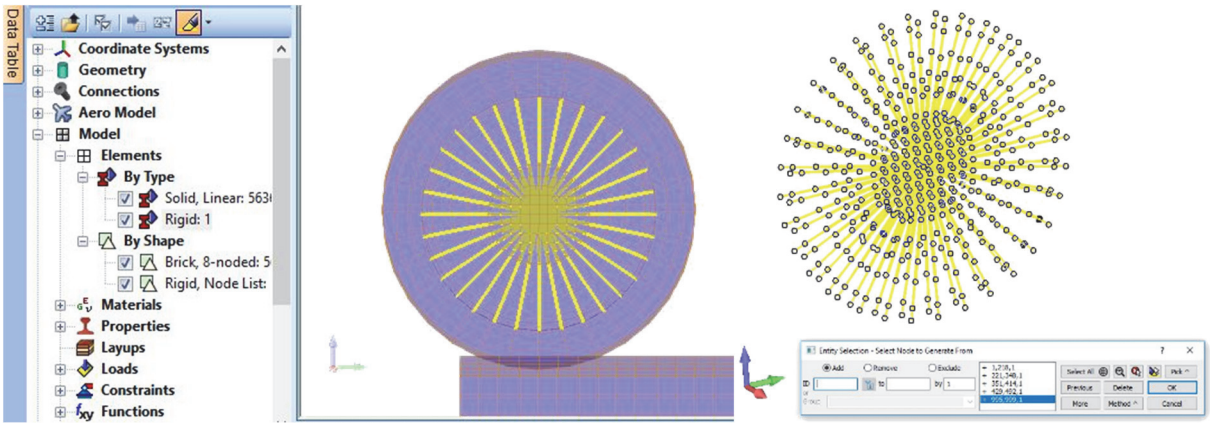

Fig.3. a) spider elements b) connecting nodes of regular beams

3. MATERIAL MODELS

3.1. Steel linear elastic rim

Linear elastic model for steel rim is characterized with Young's Modulus of 2.1e+05 MPa, Poisson's ratio of 0.3 and a density of 7.83e-03 g/mm3. Spider elements prevent any deformations of the rim, hence steel properties have no influence on model behavior and serve only to satisfy the software requirements.

3.2. Hyperelastic Mooney-Rivlin rubber tire

Tires are made of rubber composites reinforced by steel cords [10], and are studied using FEM in great detail [10], however, since our focus was primarily on asphalt, we modelled tire as a homogenous isotropic hyperelastic material. Based on test results and FEM analysis published in [10], we used Mooney-Rivlin material model with Young's Modulus of 5.05 MPa, Poisson's ratio of 0.45 and a density of 1.13e-03 g/mm3. The strain energy function of the Mooney-Rivlin model, can be expressed as:

$$W = A(I_1 - 3) + B(I_2 - 3) + C\left(\frac{1}{I_3^2} - 1\right) + D(I_3 - 1)^2 \qquad (1)$$

with:

$$C = 0.5A + B, \text{ and } D = \frac{A(5\nu - 2) + B(11\nu - 5)}{2(1 - 2\nu)} \qquad (2)$$

where ν is Poisson ratio, and I_1, I_2, I_3 are invariants of strain tensor. Material constants are: *A=0.171 MPa* and *B=0.83 MPa*.

3.3. Linear elastic, and temperature dependent elasto-viscoplastic asphalt

First we modelled asphalt as a linear viscoelastic material with dynamic Young's modulus of 7.3e+03 MPa, Poisson's ratio of 0.16 and a density of 2.22e-03 g/mm3. Young's modulus for asphalt is dependent on strain rate [2], i.e. loading frequency:

$$Log\left|E^*\right| = \delta_E \frac{\alpha_E}{1 + e^{\beta_E + \gamma_E (Log\, f_r)}} \qquad (3)$$

where $\delta_E = 1.66944$, $\alpha_E = 2.683335$, $\beta_E = -1.01996$, $\gamma_E = -0.5593$ are material parameters [2], and f_r is reduced frequency:

$$f_r = f \exp\left(a_f T^2 + b_f T + c_f\right) \qquad (4)$$

with loading frequency *f*, current temperature *T*, and material parameters $a_f = 0.0013205$ $b_f = -0.21531$, $c_f = 3.75742$.

Dynamic Young's Modulus is calculated for the lowest loading frequency of 0.1 Hz [2]. and a temperature of 20 °C. According to [11] Poisson's ratio dependence on Young's modulus for asphalt is defined by:

$$\nu = 0.15 + \frac{0.35}{1 + e^{a_\nu + b_\nu \left|E^*\right|}}, \qquad (5)$$

where coefficients have the following values: $a_\nu = -1.63$ and $b_\nu = 3.84e-6$ ($ek \equiv 10^k$). Using previously calculated dynamic Young's Modulus $\left|E^*\right|$ we get Poisson's ratio value of 0.16. Dynamic Young modulus is complex, it consists of the real part, E, corresponds to elasticity, and imaginary part, E_v, which describes viscous behavior. But, for very low frequency *f*, Dynamic Young modulus coincides with its real part.

For long-term analysis of asphalt behavior and failure prediction (shown on Figure 2.b) we needed temperature dependent elasto-viscoplastic material model. We have extended model presented in [3] with temperature dependent material parameters. This model is based on Perzyna's theory of viscoplasticity in which yield surface is given by dynamic loading function [12]. The strain energy function, for asphalt reads:

$$W = \left(A_5 I_1^2 + A_1 I_2\right) + A_3 I_1^3 + A_4 I_1 I_2 + A_2 I_3 \qquad (6)$$

where I_1, I_2, I_3 are proper invariants of the elastic strain $\boldsymbol{\varepsilon}^e$ [1], and $A_1 = 3.6e3$, $A_2 = -0.6046e5$, $A_3 = -1.81e5$, $A_4 = -0.906e5$, $A_5 = 70.3e2$ are material parameters [3]. Trial stress tensor is calculated as a partial derivative of *W* with respect to $\boldsymbol{\varepsilon}^e$:

$$\boldsymbol{\sigma} = \frac{\partial W\left(\boldsymbol{\varepsilon}^e\right)}{\partial \boldsymbol{\varepsilon}^e} \quad \Rightarrow \quad \boldsymbol{\sigma} = \left(2A_5 I_1 + 3A_3 I_1^2 + A_4 I_2\right)\mathbf{1} + \left(A_1 + A_4 I_1\right)\boldsymbol{\varepsilon}^e + A_2\left(\boldsymbol{\varepsilon}^e\right)^2 \tag{7}$$

which is then used to test if the stress state is within elastic or plastic range. The loading function is:

$$f = \left|\bar{S}_1 \bar{S}_2 + \alpha_s \bar{S}_3\right| - H\kappa \tag{8}$$

Here, $H = 50$ and $a_s = 14.2$ are material parameters, and the first, second and the third stress invariants are calculated as $\bar{S}_1 = tr\boldsymbol{\sigma}$, $\bar{S}_2 = \left(tr\boldsymbol{\sigma}_d^2 - \bar{S}_1^2\right)/2$, $\bar{S}_3 = \det \boldsymbol{\sigma}_d$, using deviatoric stress tensor $\boldsymbol{\sigma}_d$ [1]. The hardening variable κ and the evolution equation for the viscoplastic strain are calculated as:

$$\dot{\kappa} = \left(\frac{\langle f \rangle}{\eta}\right)^m \frac{1}{x + \kappa^l}, \qquad \dot{\boldsymbol{\varepsilon}}^{vp} = \left(\frac{\langle f \rangle}{\eta}\right)^m \frac{1}{x + \kappa^l}\mathbf{v} \equiv \dot{\kappa}\mathbf{v} \tag{9}$$

where Macaulay brackets $\langle\ \rangle$ denote ramp function $\langle y \rangle = (y + |y|)/2$, and $\eta = 1.34e9$, $x = 1.03$, $l = 2.2$, $m = 1$ are material parameters. Normal to the viscoplastic loading surface $\mathbf{v} = \frac{\boldsymbol{\sigma}_d}{2\sqrt{J_2}} + \gamma\mathbf{1}$ is calculated using the second invariant of the deviatoric stress tensor $J_2 = tr\,\boldsymbol{\sigma}_d^2/2$ and material parameter $\gamma = -0.05$.

These equations serve for predictor-corrector algorithm in which first we calculate trial stress tensor (eq. 7.), then we check if the plasticity condition is satisfied (eq. 8.). In case of elasticity we move on to the next step, but in case of plasticity, we move into corrector phase in which we iteratively increase hardening variable and viscoplastic strain (eq. 9.). Increase of viscoplastic strain leads to reduction of elastic strain in that iteration $\boldsymbol{\varepsilon}_{n+1}^{e(k+1)} = \boldsymbol{\varepsilon}_{n+1} - \boldsymbol{\varepsilon}_{n+1}^{vp(k+1)} - \boldsymbol{\varepsilon}_{n+1}^{th(k+1)}$ so the trial stress tensor (eq. 7.) needs to be reevaluated. Thermal strains $\boldsymbol{\varepsilon}_{n+1}^{th(k+1)} = \alpha_T \vartriangle T\mathbf{1}$ are calculated using thermal expansion coefficient α_T and temperature difference $\vartriangle T$. These iterations continue until the increments $\kappa_{n+1}^{(k+1)} - \kappa_{n+1}^{(k)}$ or $\boldsymbol{\varepsilon}_{n+1}^{vp(k+1)} - \boldsymbol{\varepsilon}_{n+1}^{vp(k)}$ are less than tolerance.

4. RESULTS AND DISCUSSION

Figure 4 shows Von Misses stress at the beginning and at the end of rolling.

Fig.4. Von Misses stress [MPa] a) at t=0s b) at t=1s

As it can be seen from the Figure 4 deformations of the tire are far greater than deformations of the asphalt, so in the Figure 5, we will show only vertical translation in the asphalt (with particular focus on node N on asphalt surface).

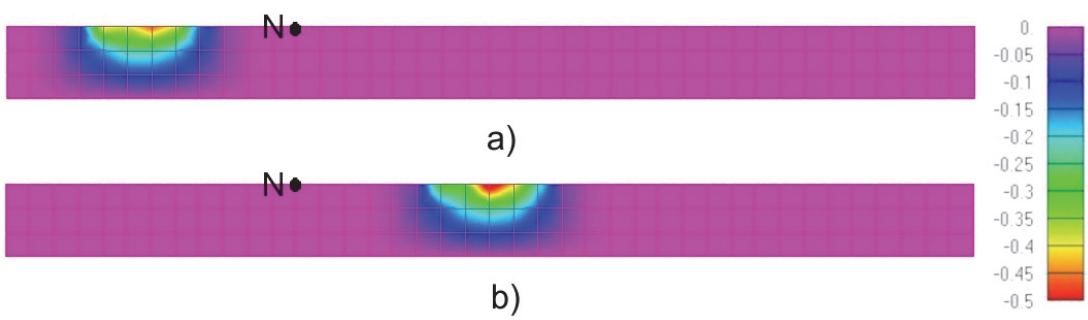

Fig.5. Vertical displacement [mm] a) at t=0s b) at t=1s

Due to asphalt viscosity, lower rates of deformation cause more permanent damage, so most of the rooting occurs near intersections where traffic is the slowest and the rate of deformation lowest. Therefore, we prescribed velocity of 0.8 m/s or 2.88 km/h and obtain vertical displacement over time of a node N as the wheel passes over it. We can

track this vertical displacement throughout the analysis, (Figure 6.a), and later, we can use it as a loading function of prescribed displacement in the FEM model of test cylindrical (Figure 6.b).

The middle of the wheel crosses over observed node at 0.6 seconds, so that is the time of the largest vertical displacement. We can also see that at 0.2 seconds, and after 0.8 seconds, the vertical displacement is positive, as the node at these times belongs to the excess volume of the asphalt that the wheel pushes out of the pavement.

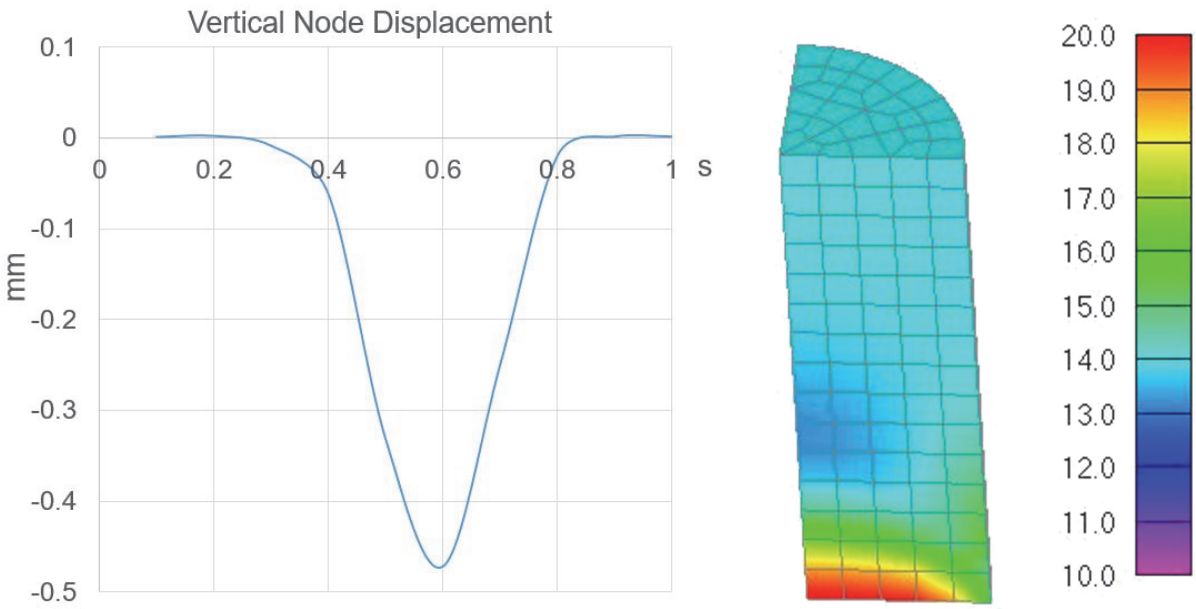

a) *b)*

Fig.6. a) Vertical displacement of node N (from eqs. (3)-(5))
b) Von Misses stress [MPa] in FEM model of asphalt specimen from PAK induced by this displacement (for material model defined by eqs, (6)-(9))

5. CONCLUSION

Prediction of elasto-viscoplastic response of asphalt requires a material model dependent on temperature, as well as realistic loading function. In this paper, we have shown FEM modelling of tire rolling over the asphalt pavement with boundary conditions that gave us insight into the interaction between the wheel and the asphalt. Afterwards, we used this result as a loading function in a simplified FEM model representing the experimental cylindrical specimen found in the literature. We will use this FEM model in our future research which will be focused on analysis of elasto-viscoplastic material model parameters, their dependence on the temperature and rate of deformation.

ACKNOWLEDGEMENT

This research is supported by the Ministry of Education, Science and Technological Development, Republic of Serbia, Grant TR32036 and 451-03-68/2020-14/200378.

REFERENCES

[1] Micunovic, M. (2009). *Thermomechanics of Viscoplasticity - Fundamentals and Applications*, Springer, New York.

[2] Kirukhin, G. (2016). *Reversible Deformation of Asphalt Concrete Depending on Loading Conditions*, LLC Institute of Road Pavement, Moscow.

[3] Panneerselvam, D. (2005). *Mechanics of Asphalt Concrete: Analytical and Computational Studies*, PhD thesis, Department of Civil Engineering, Case Western Reserve University, Cleveland, Ohio.

[4] Mitra K., Das A., Basu S. (2012). Mechanical behavior of asphalt mix: An experimental and numerical study. *Construction and Building Materials*, vol. 27, p.p. 545–552.

[5] Topalovic, M. (2016). *Numerical modelling of granular materials*, (in Serbian), PhD thesis, Faculty of Engineering, University of Kragujevac, Kragujevac.

[6] Bahuguna, S., Panoskaltsis V., Papoulia K. (2006). Identification and Modeling of Permanent Deformations of Asphalt Concrete, *Journal of Engineering Mechanics*, vol. 132, p.p. 231-239.

[7] Vulović, S., Bojović, M., Topalović, M. (2020) *Automation of FEM Analysis Report Generation using Visual Basic FEMAP API*. ICIST 2020 Proceedings vol.1, pp.10-15.

[8] Kudrjavceva, L., Mićunović, M., Topalović, M., Sedmak S. (2014). *Thermomechanics of Soft Inelastics Bodies with Application to Asphalt Behavior*, Thermal Science, vol. 18, pp. S221-S228.

[9] Kojić, M., Slavković, R., Živković M., Grujović, N. (1998). *Metod konačnih elemenata I, Linearna*

analiza, Kragujevac: Mašinski fakultet, Univerzitet u Kragujevcu.

[10] Baranowski, P., Bogusz, P.,Gotowicki, P., Małachowski, J. (2012). Assessment Of Mechanical Properties Of Offroad Vehicle Tire: Coupons Testing And Fe Model Development, *Acta Mechanica et Automatica*, vol.6. no.2. pp. 17-22.

[11] Islam R., Faisal H., Tarefder R. (2015). Determining temperature and time dependent Poisson's ratio of asphalt concrete using indirect tension test, *Fuel*, vol. 146, pp. 119-124.

[12] Perzyna P., (1966). Fundamental Problems in Viscoplasticity, *Advances in Applied Mechanics*, vol. 9, pp. 243–377.